Supplementary Information: Plasmonic Characteristics of the Structure with Double Graphene Layers Immersed in Chiral Media and Applications in Detection of Chirality†

Rui Zhao, Xingguang Liu, Junqing Li* and Yingjie Zhang

1 The Derivation for the Universal Dispersion Relation with Setting Chirality as Zero

By Bohren decomposition, the primary electric and magnetic fields in the chiral medium are retrieved from[1]

$$\begin{aligned}\mathbf{E} &= (\mathbf{F}_+ + \mathbf{F}_-)/2 \\ \mathbf{H} &= (\mathbf{F}_+ - \mathbf{F}_-)/(2\mathrm{i}\eta).\end{aligned} \tag{1}$$

$$M = \begin{bmatrix}
-1 & -1 & 1 & 1 & e^{-d\alpha_{2+}} & e^{-d\alpha_{2-}} & 0 & 0 \\
\frac{\alpha_{1+}}{k_{1+}} & -\frac{\alpha_{1-}}{k_{1-}} & \frac{\alpha_{2+}}{k_{2+}} & -\frac{\alpha_{2-}}{k_{2-}} & -\frac{\alpha_{2+}}{k_{2+}}e^{-d\alpha_{2+}} & \frac{\alpha_{2-}}{k_{2-}}e^{-d\alpha_{2-}} & 0 & 0 \\
\left(-\frac{\mathrm{i}}{\eta_1}+\sigma\frac{\alpha_{1+}}{k_{1+}}\right) & \left(\frac{\mathrm{i}}{\eta_1}-\sigma\frac{\alpha_{1-}}{k_{1-}}\right) & \frac{\mathrm{i}}{\eta_2} & -\frac{\mathrm{i}}{\eta_2} & \frac{\mathrm{i}}{\eta_2}e^{-d\alpha_{2+}} & -\frac{\mathrm{i}}{\eta_2}e^{-d\alpha_{2-}} & 0 & 0 \\
\left(-\sigma-\frac{\mathrm{i}\alpha_{1+}}{\eta_1 k_{1+}}\right) & \left(-\sigma-\frac{\mathrm{i}\alpha_{1-}}{\eta_1 k_{1-}}\right) & -\frac{\mathrm{i}\alpha_{2+}}{\eta_2 k_{2+}} & -\frac{\mathrm{i}\alpha_{2-}}{\eta_2 k_{2-}} & \frac{\mathrm{i}\alpha_{2+}}{\eta_2 k_{2+}}e^{-d\alpha_{2+}} & \frac{\mathrm{i}\alpha_{2-}}{\eta_2 k_{2-}}e^{-d\alpha_{2-}} & 0 & 0 \\
0 & 0 & e^{-d\alpha_{2+}} & e^{-d\alpha_{2-}} & 1 & 1 & -1 & -1 \\
0 & 0 & -\frac{\alpha_{2+}}{k_{2+}}e^{-d\alpha_{2+}} & \frac{\alpha_{2-}}{k_{2-}}e^{-d\alpha_{2-}} & \frac{\alpha_{2+}}{k_{2+}} & -\frac{\alpha_{2-}}{k_{2-}} & \frac{\alpha_{3+}}{k_{3+}} & -\frac{\alpha_{3-}}{k_{3-}} \\
0 & 0 & -\frac{\mathrm{i}k_{2+}+\eta_2\sigma\alpha_{2+}}{\eta_2 k_{2+}}e^{-d\alpha_{2+}} & \frac{\mathrm{i}k_{2-}+\eta_2\sigma\alpha_{2-}}{\eta_2 k_{2-}}e^{-d\alpha_{2-}} & \frac{-\mathrm{i}k_{2+}+\eta_2\sigma\alpha_{2+}}{\eta_2 k_{2+}} & \frac{\mathrm{i}k_{2-}-\eta_2\sigma\alpha_{2-}}{\eta_2 k_{2-}} & \frac{\mathrm{i}}{\eta_3} & -\frac{\mathrm{i}}{\eta_3} \\
0 & 0 & -\frac{\eta_2\sigma k_{2+}-\mathrm{i}\alpha_{2+}}{\eta_2 k_{2+}}e^{-d\alpha_{2+}} & -\frac{\eta_2\sigma k_{2-}-\mathrm{i}\alpha_{2-}}{\eta_2 k_{2-}}e^{-d\alpha_{2-}} & \left(-\sigma-\frac{\mathrm{i}\alpha_{2+}}{\eta_2 k_{2+}}\right) & \left(-\sigma-\frac{\mathrm{i}\alpha_{2-}}{\eta_2 k_{2-}}\right) & -\frac{\mathrm{i}\alpha_{3+}}{\eta_3 k_{3+}} & -\frac{\mathrm{i}\alpha_{3-}}{\eta_3 k_{3-}}
\end{bmatrix} \tag{2}$$

Utilizing trigexpand and setting $\kappa_1 = \kappa_2 = \kappa_3 = 0$, which means that $\alpha_{1\pm,3\pm} = \alpha,\ k_{1\pm,3\pm} = k,\ \eta_1 = \eta_3 = \eta$, the universal dispersion relation $|M| = 0$ can be reduced to:

$$\begin{aligned}&\left[\alpha_2\eta_2\left(k+\mathrm{i}\alpha\eta\sigma\right)\cosh\frac{d\alpha_2}{2}+k_2\alpha\eta\sinh\frac{d\alpha_2}{2}\right]\left[k_2\eta_2\left(\alpha-\mathrm{i}k\eta\sigma\right)\cosh\frac{d\alpha_2}{2}+k\alpha_2\eta\sinh\frac{d\alpha_2}{2}\right] \\ &\left[k_2\eta_2\left(\alpha-\mathrm{i}k\eta\sigma\right)\sinh\frac{d\alpha_2}{2}+k\alpha_2\eta\cosh\frac{d\alpha_2}{2}\right]\left[\alpha_2\eta_2\left(k+\mathrm{i}\alpha\eta\sigma\right)\sinh\frac{d\alpha_2}{2}+k_2\alpha\eta\cosh\frac{d\alpha_2}{2}\right]=0.\end{aligned} \tag{3}$$

Multiplying Eq. 3 by $1/(\alpha_2\eta_2\alpha\eta)$ and substituting the relation of

$$\begin{aligned}k/\eta &= \frac{\omega\sqrt{\varepsilon_0\mu_0\varepsilon_r}}{\sqrt{\mu_0/(\varepsilon_0\varepsilon_r)}} = \omega\varepsilon_0\varepsilon_r, \\ k\eta &= \omega\sqrt{\varepsilon_0\mu_0\varepsilon_r}\sqrt{\mu_0/(\varepsilon_0\varepsilon_r)} = \omega\mu_0, \\ k_2/\eta_2 &= \frac{\omega\sqrt{\varepsilon_0\mu_0\varepsilon_{r2}}}{\sqrt{\mu_0/(\varepsilon_0\varepsilon_{r2})}} = \omega\varepsilon_0\varepsilon_{r2}, \\ k_2\eta_2 &= \omega\sqrt{\varepsilon_0\mu_0\varepsilon_{r2}}\sqrt{\mu_0/(\varepsilon_0\varepsilon_{r2})} = \omega\mu_0,\end{aligned} \tag{4}$$

into the Eq. 3, we can derive the dispersion relation as:

$$\begin{aligned}&\left[\left(\frac{\varepsilon_r}{\alpha}+\frac{\mathrm{i}\sigma}{\omega\varepsilon_0}\right)\cosh\left[\frac{\alpha_2 d}{2}\right]+\frac{\varepsilon_2}{\alpha_2}\sinh\left[\frac{\alpha_2 d}{2}\right]\right]\left[\left(\alpha-\mathrm{i}\omega\mu_0\sigma\right)\cosh\left[\frac{\alpha_2 d}{2}\right]+\alpha_2\sinh\left[\frac{\alpha_2 d}{2}\right]\right] \\ &\left[\left(\alpha-\mathrm{i}\omega\mu_0\sigma\right)\sinh\left[\frac{\alpha_2 d}{2}\right]+\alpha_2\cosh\left[\frac{\alpha_2 d}{2}\right]\right]\left[\left(\frac{\varepsilon_r}{\alpha}+\frac{\mathrm{i}\sigma}{\omega\varepsilon_0}\right)\sinh\left[\frac{\alpha_2 d}{2}\right]+\frac{\varepsilon_{r2}}{\alpha_2}\cosh\left[\frac{\alpha_2 d}{2}\right]\right]=0.\end{aligned} \tag{5}$$

[a] Xidazhi Street NO.29, Harbin, China.
* Junqing Li. E-mail: jqli@hit.edu.cn

Next let us start from the dispersion relation of TM-SPPs in the achiral structure with double graphene sheets:

$$AA = \det\begin{bmatrix} -1 & 1 & 1 & 0 \\ \frac{\varepsilon_{r3}}{\alpha_3}+\frac{i\sigma}{\omega\varepsilon_0} & -\frac{\varepsilon_{r2}}{\alpha_2} & \frac{\varepsilon_{r2}}{\alpha_2} & 0 \\ 0 & \frac{\varepsilon_{r2}}{\alpha_2}e^{d\alpha_2} & -\frac{\varepsilon_{r2}}{\alpha_2}e^{-d\alpha_2} & \left(\frac{i\sigma}{\omega\varepsilon_0}+\frac{\varepsilon_{r1}}{\alpha_1}\right)e^{-d\alpha_1} \\ 0 & e^{d\alpha_2} & e^{-d\alpha_2} & -e^{-d\alpha_1} \end{bmatrix} = 0. \tag{6}$$

When considering $\alpha_1 = \alpha_3,\ \varepsilon_{r1} = \varepsilon_{r3}$, we can get:

$$\begin{aligned} &\left(\frac{\varepsilon_{r3}}{\alpha_3}+\frac{\varepsilon_{r2}}{\alpha_2}+\frac{i\sigma_g}{\omega\varepsilon_0}\right)\left(\frac{\varepsilon_{r3}}{\alpha_3}+\frac{\varepsilon_{r2}}{\alpha_2}+\frac{i\sigma_g}{\omega\varepsilon_0}\right)e^{\alpha_2 d} = \\ &\left(\frac{\varepsilon_{r3}}{\alpha_3}-\frac{\varepsilon_{r2}}{\alpha_2}+\frac{i\sigma_g}{\omega\varepsilon_0}\right)\left(\frac{\varepsilon_{r3}}{\alpha_3}-\frac{\varepsilon_{r2}}{\alpha_2}+\frac{i\sigma_g}{\omega\varepsilon_0}\right)e^{-\alpha_2 d} \end{aligned} \tag{7}$$

According to the reference,[2,3] the Eq. 6 can be derived as

$$\begin{aligned} &\left[\left(\frac{\varepsilon_r}{\alpha}+\frac{i\sigma}{\omega\varepsilon_0}\right)\cosh\left[\frac{\alpha_2 d}{2}\right]+\frac{\varepsilon_2}{\alpha_2}\sinh\left[\frac{\alpha_2 d}{2}\right]\right] \\ &\left[\left(\frac{\varepsilon_r}{\alpha}+\frac{i\sigma}{\omega\varepsilon_0}\right)\sinh\left[\frac{\alpha_2 d}{2}\right]+\frac{\varepsilon_{r2}}{\alpha_2}\cosh\left[\frac{\alpha_2 d}{2}\right]\right] = 0, \end{aligned} \tag{8}$$

One can see the first and fourth factors of Eq. 5 are the same as Eq. 8, namely the dispersion of TM-SPPs in achiral case. Analogously, the second and third factors of Eq. 5 are the dispersion of TE-SPPs in achiral case. Thus, we argue that there is no conflict between Eq. 3 and Eq. 8. About the intelligence about the TE-SPPs, one can refer to the literature.[4] Note that we take the nonmagnetic material ($\mu_r = 1$) during the entire procession.

We can explain the physical insights of the evolution of the dispersion relation. The hybrid plamonic modes in CGCGC structure, which can be described by $|M| = 0$, are different from the pure TM and TE modes in the structure without chirality. When the chirality is reduced to zero, the dispersion relation reduces to the product of the TM and TE contributions, which generalise the traditional dispersion relation of the SPPs in the structure without chirality and with double graphene layers.

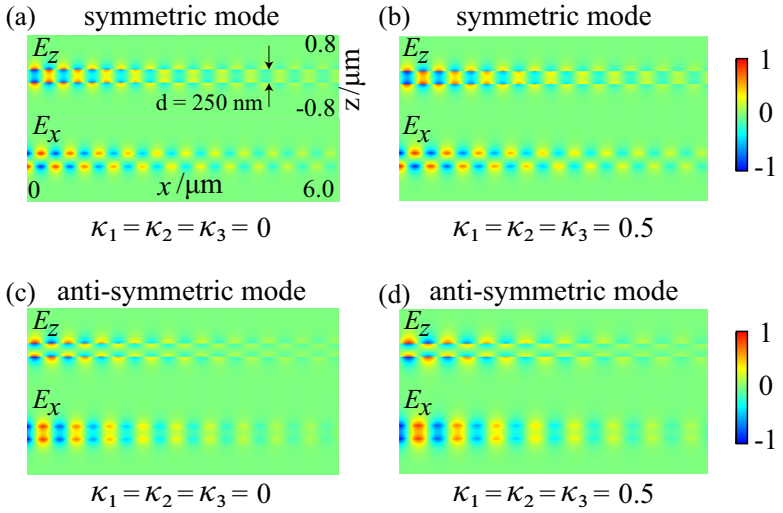

Fig. 1 The dependence propagation constant of symmetric mode and anti-symmetric mode in achiral and chiral cases with $\varepsilon_{r1} = \varepsilon_{r2} = \varepsilon_{r3} = 2$.

The distributions of E_z and E_x for symmetric mode and anti-symmetric modes are presented in Fig. 1 (one is symmetric then the other anti-symmetric), which corresponds to the excitation frequency at the intersections of the white dotted line with dispersion curves in Fig.2 in the article. Besides, the third field component E_y, which is far less than E_z and E_x components, is unzero in chiral cases but zero in achiral cases. The distribution of fields

is extended and the propagation is improved slightly.

2 Discussion on the Dispersion Relation

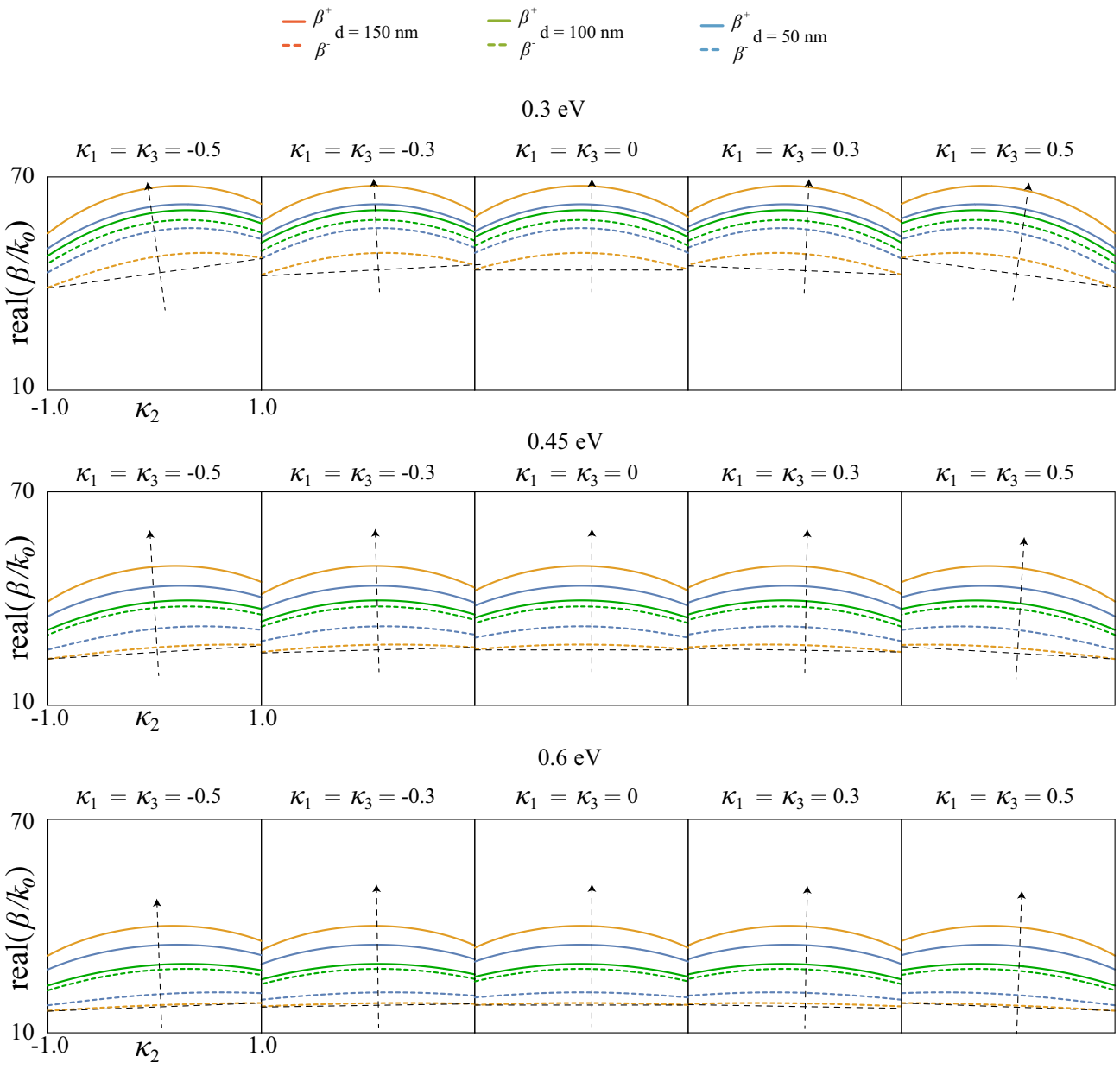

Fig. 2 The dependence of propagation constant of symmetric mode (β^+) and anti-symmetric mode (β^-) on κ_2 and $\varepsilon_{r1} = \varepsilon_{r2} = \varepsilon_{r3} = 2$.

In the case of $\kappa_1 = \kappa_3 = 0$, the variation of propagation constant with the chirality in core medium shows a symmetric arch tendency, while in the case of $\kappa_1 = \kappa_3 \neq 0$, the tendency become asymmetrically inclined and the inclining direction depends on the sign of the chirality of the environment. It seems that there exists a calibration effect of chirality in core medium on the chirality of environment. We exhibit the propagation constant with different chemical potential of graphene (0.3 eV, 0.45 eV, 0.6 eV) and the chirality of medium 1, 3 (0, $\pm$0.3, $\pm$0.5) as the chirality of medium 2 sweeps ranging from -1 to 1 as shown in Fig. 2.

Fig. 3 demonstrates the relations between the propagation constant β and the chemical potential of graphene μ_c with and without chirality in three typical distances between two graphene sheets according to the dispersion of GSPPs in CGC structure under the wavelength of 10 μm. It is clear that the propagation constant decreases with the increase of chemical potential of graphene and becomes flattened gradually for larger μ_c. Also, the graphene with a small chemical potential is not a reliable material for exciting GSPPs. In this case, the effective

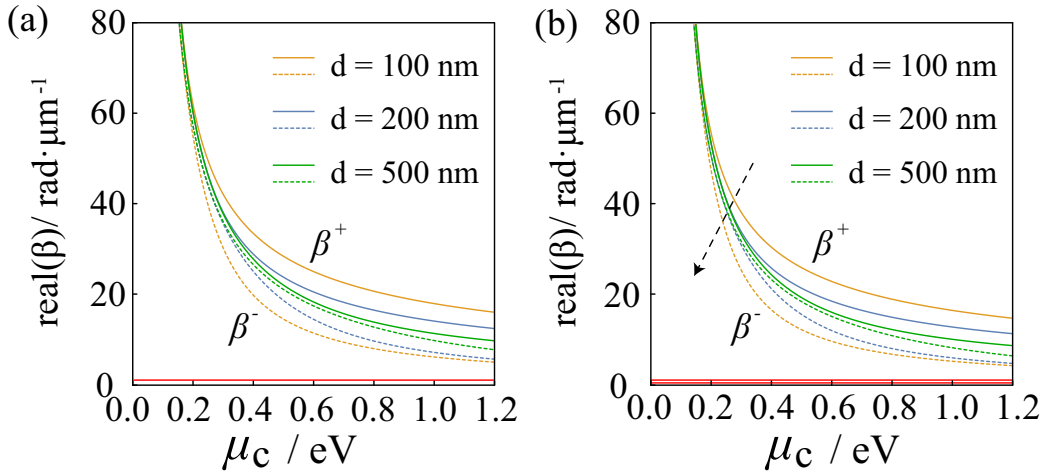

Fig. 3 The dependence propagation constant of symmetric mode (β_+) and anti-symmetric mode (β_-) on μ_c and $\varepsilon_{r1} = \varepsilon_{r2} = \varepsilon_{r3} = 2,\ \kappa_1 = \kappa_2 = \kappa_3 = 0$ in (a) and $\kappa_1 = \kappa_2 = \kappa_3 = 0.5$ in (b).

wavelength approaches 0, the effective refractive index is meaningless and there exist neither symmetric mode nor anti-symmetric mode. Compared with the achiral case, the minimum chemical potential to excite the GSPPs becomes smaller in the chiral case. The chirality plays a more important role in an appropriate distance between the two graphene sheets. In the case of large distance without chiral medium, the interaction of GSPPs near two graphene sheets is weak, which results in the trivial splitting of the curves, depicting the relation between β and μ_c (see the solid and dashed green lines in Fig. 3). After the introduction of chirality, the interaction is enhanced and the curve difference becomes larger. By contrast, the influence of chirality in a smaller distance is concealed by the effect of distance. It should be pointed that there is only one line at the bottom of Fig. 3 (a), but two lines in Fig. 3 (b), which correspond to the dielectric line splitting mentioned in the manuscript.

3 Interpretation of the Formulas of Optical Force and Torque

Considering the configuration shown in Fig. 4 (a), the particle (sphere) with radius $r = 50$ nm and $\varepsilon_{sp} = 2$ is placed in the core of the structure as the detector particle. Then we investigate the optical force and torque exerted on the particle. In fact, when the size of the particle is much smaller than the wavelength, namely in the Rayleigh regime, $kr \ll 1$, the problem can be simplified as the dipole approximation. Without loss of generality, we take an example of symmetric mode with $\mu_c = 0.30$ eV, $\lambda = 15$ μm.

The induced dipolar moments of such a chiral particle can be expressed as:

$$\begin{bmatrix} \mathbf{p} \\ \mathbf{m} \end{bmatrix} = \begin{bmatrix} \alpha_{ee} & \mathrm{i}\alpha_{em} \\ -\mathrm{i}\alpha_{em} & \alpha_{mm} \end{bmatrix} \begin{bmatrix} \mathbf{E} \\ \mathbf{H} \end{bmatrix}, \tag{9}$$

where $\mathbf{p}$ and $\mathbf{m}$ are the electric and magnetic moments, respectively; $\mathbf{E}$ and $\mathbf{H}$ are the fields acting on the particle. Here the polarizability of the particle is specified by parameters α_{ee}, α_{mm} and α_{em}. Note that, the particle we introduced is achiral, namely $\alpha_{em} = 0$. The generalized expression of the optical force based on the dipole approximation writes as[5]:

$$\begin{aligned} \mathbf{F} =& \nabla U + \sigma \frac{\mathbf{S}_w}{c} - \mathbf{Im}\left[\alpha_{em}\right] \nabla \times \mathbf{S}_w + c\sigma_e \times \mathbf{L_e} + c\sigma_m \times \mathbf{L_m} \\ &+ \omega \gamma_e \mathbf{L_e} + \omega \gamma_m \mathbf{L_m} + \frac{c k_{spp}^4}{12\pi} \mathbf{Im}\left[\alpha_{ee} \alpha_{mm}^*\right] \mathbf{Im}\left[\mathbf{E} \times \mathbf{H}^*\right]. \end{aligned} \tag{10}$$

The first and second terms in the equation above represent the gradient force and radiation pressure, and the remaining terms describe the scattering recoil force.

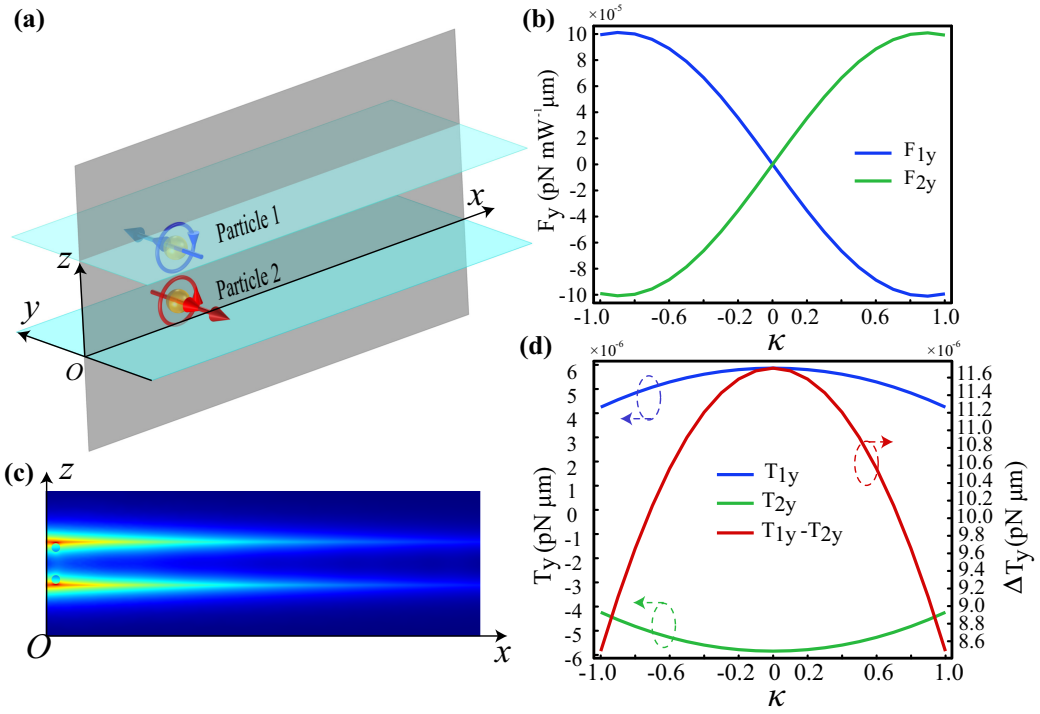

Fig. 4 Force and torque symmetric mode of SPPs. (a) The schematic of detecting the chirality in the environment. (b) The lateral force versus κ. (c) The side view of norm electric field in the structure. (c) The lateral torque versus κ. $\lambda = 15$ μm, $d = 300$ nm, $\mu_c = 0.30$ eV, $\varepsilon_{r1} = \varepsilon_{r3} = 2.25$, $\varepsilon_{r2} = 1$, and $\kappa_1 = \kappa_3 = \kappa$, $\kappa_2 = 0$.

$$
\begin{aligned}
U &= 1/4\left(\mathbf{Re}\left[\alpha_{ee}\right]|\mathbf{E}|^2 + \mathbf{Re}\left[\alpha_{mm}\right]|\mathbf{H}|^2 - 1/2\mathbf{Re}\left[\alpha_{em}\right]\mathbf{Im}\left[\mathbf{H}\cdot\mathbf{E}\right]\right),\\
\mathbf{S}_w &= \tfrac{1}{2}\mathbf{Re}\left[\mathbf{E}\times\mathbf{H}^*\right],\quad \mathbf{L_e} = \tfrac{i\varepsilon_0}{4\omega\mu_r}\mathbf{E}\times\mathbf{E}^*,\quad \mathbf{L_m} = \tfrac{i\mu_0}{4\omega\varepsilon_r}\mathbf{H}\times\mathbf{H}^*,\\
\sigma_e &= \tfrac{k_{spp}}{\varepsilon_0}\mathbf{Im}\left[\alpha_{ee}\right],\quad \sigma_m = \tfrac{k_{spp}}{\mu_0}\mathbf{Im}\left[\alpha_{mm}\right],\quad \sigma_t = \sigma_e + \sigma_m - \tfrac{c^2k_{spp}^4}{6\pi}\left(\mathbf{Re}\left[\alpha_{ee}\alpha_{mm}^*\right] + \alpha_{em}\alpha_{em}^*\right),\\
\gamma_e &= -2\omega\mathbf{Im}\left[\alpha_{em}\right] + \tfrac{ck_{spp}^4}{3\pi\varepsilon_0}\mathbf{Im}\left[\alpha_{ee}\alpha_{em}^*\right],\quad \gamma_m = -2\omega\mathbf{Im}\left[\alpha_{em}\right] + \tfrac{ck_{spp}^4}{3\pi\varepsilon_0}\mathbf{Im}\left[\alpha_{mm}\alpha_{em}^*\right].
\end{aligned}
\tag{11}
$$

U is the term due to particle–field interaction; $\mathbf{S}_w$ stand for the time average energy density, electric spin angular momentum density, and magnetic spin angular momentum density respectively. σ_e, σ_m, and σ_t are the cross-section. In addition, γ_e and γ_m also have the dimension of a cross-section. And the generalized expression of the optical torque writes as[6,7]:

$$
\mathbf{T} = \mathrm{Re}\left[\alpha_{em}^*\right]\mathbf{S} - \frac{2\omega}{\varepsilon_0}\mathrm{Re}\left[\alpha_{ee}^*\right]\mathbf{L_e} - \frac{2\omega}{\varepsilon_0}\mathrm{Re}\left[\alpha_{mm}^*\right]\mathbf{L_m}. \tag{12}
$$

References

1 Y. Cao and J. Li, *Phys. Rev. B*, 2014, **89**, 115420.

2 Y. V. Bludov, A. Ferreia, N. M. R. Peres and M. I. Vasilevskiy, *International Journal of Modern Physics B*, 2013, **27**, 1341001.

3 P. A. D. Gonçalves and N. M. R. Peres, *An Introduction to Graphene Plasmonics*, WORLD SCIENTIFIC, 2016.

4 A. Vakil and N. Engheta, *Science*, 2011, **332**, 1291–1294.

5 S. Wang and C. Chan, *Nat Commun*, 2014, **5**, 1–8.

6 A. Canaguier-Durand, J. A. Hutchison, C. Genet and T. W. Ebbesen, *New Journal of Physics*, 2013, **15**, 123037.

7 V. Svak, O. Brzobohatý, M. Šiler, P. Jákl, J. Kaňka, P. Zemánek and S. H. Simpson, *Nat Commun*, 2018, **9**, 5453.